On the Relation between X-Ray Diffraction Angle and Atomic Spacing in Metallic Glasses

Xinwei YE [1], Jianjun PANG[1, 2] *, Xinyi ZUO [1], Feng LIU [1], Yadong LI [1]

[1] *School of Mechanical Engineering, Zhejiang University of Water Resources and Electric Power, Hangzhou 310018, Zhejiang, China*
[2] *Zhejiang Engineering Research Center of Advanced Water Conservancy Equipment, Hangzhou 310018, Zhejiang, China*

http://doi.org/10.5755/j02.ms.42751

Received 9 September 2025; accepted 5 January 2026

The Bragg equation, which is usually employed to calculate the lattice constants of crystals, cannot be directly applied to amorphous alloys because they do not sustain long-range periodicity. A correction factor has to be involved, and the Debye equation predicts this to have a value of 1.23. Here, the amorphous structure of metallic glasses is investigated with XRD (Cu *K*α) and the diffraction angle where the broad amorphous peak emerges is shown to be dependent on composition. By fitting the data of the dependence of the average atomic spacing on $\lambda/(2\sin\theta)$, a factor of 1.22 was attained for metallic glasses with predominantly metallic bonding character, and even lower values if considerable covalent-like bonding is present. The lower factor can be explained by denser atomic packing in real amorphous metallic systems compared to that predicted by the random packing model.
Keywords: metallic glasses, Debye equation, random packing, X-ray diffraction, atomic packing efficiency.

1. INTRODUCTION

Metallic glasses (MGs) are widely known due to their peculiar thermal and mechanical properties as compared to their crystalline forms [1, 2]. These unique properties result from their unique structures. As the name suggests, MGs have a glasslike amorphous structure at the atomic level and thus do not show crystalline periodicity, which can be distinguished by using X-ray diffraction (XRD) techniques. Unlike the XRD spectra of crystals, which are characterized by multiple narrow and sharp diffraction peaks, the MGs' are usually made of a few broad diffraction peaks with damping intensities at high scattering angles. Hence, it is necessary to make it clear what the diffraction angle indicates in this work. The so-called diffraction angle of this study is measured using Cu *K*α X-ray and corresponds to that where the maximum intensity of the first diffuse halo takes place. This position is related to the interatomic distances, i.e., as the position is obtained, the distance between atom pairs can be estimated.

High-energy synchrotron XRD is commonly used to generate high-resolution spectra [2-4]. However, this technique is not easily accessible in terms of experimental operation and data analysis. Instead, conventional XRD with radiation from pure metals (most commonly Cu) is one simple avenue for calculating the average bonding length (*i.e.*, interatomic distance between adjacent atoms). For example, Senkov et al. [5], by means of XRD diffraction with Cu *K*α radiation, computed the average bonding length of Ca-Mg-Cu glasses with the Bragg equation. When compared to the metallic and covalent radii of atoms, the bonding characters can be more or less identified [5-7]. It should be noticed that the Bragg equation is derived for crystalline materials, while MGs do not have long-range order and thus a correction on the Bragg equation should be made so as to correctly reflect the average interatomic distance.

This work investigates the relation between the diffraction angle and the average atomic distance. To this end, some glassy alloys such as Al-, Mg-, La-, Zr- and Cu-based types were chosen, and their structural properties were measured by conventional X-ray diffraction. The data on atom-pair distances are extracted from the literature.

2. THEORY

In fact, amorphous diffraction theory has long been developed by Debye [8] who formulated the X-ray scattering intensity for a system of N atoms as:

$$I(k) = \sum_{i=1}^{N}\sum_{j=1}^{N} f_i f_j \frac{\sin(2\pi k \cdot r_{ij})}{2\pi k r_{ij}}, \quad (1)$$

where r_{ij} is the distance between the i_{th} and j^{th} atoms; f_i and f_j is the respective atomic scattering factor; k is the scattering vector with its value of $(2\sin\theta/\lambda)$; θ is the scattering angle, λ is the X-ray wavelength. The intensity is due to the interaction of one atom with itself, and as well the interaction between the i_{th} and j_{th} atoms. In addition, the latter interaction is calculated twice. By assuming only one type of atom, Eq.1 can be written [9]:

$$I(k) = Nf^2 + 2f^2\sum\frac{\sin(2\pi k \cdot r)}{2\pi k r} = Nf^2\left[1 + \frac{2}{N}\sum\frac{\sin(2\pi k \cdot r)}{2\pi k r}\right], \quad (2)$$

where f is the atomic scattering factor; r is the interatomic distance. Without considering the dependence of f on the scattering angle θ, the first intensity maxima, which is

* Corresponding author: J. Pang
E-mail: *pangjj@zjweu.edu.cn*

related to the average radius R_{avg} of the first coordination shell [8, 9], is obtained by letting the derivative of Eq. 2 equal to zero:

$$kr = \frac{2\sin\theta}{\lambda} \cdot r = 1.23; \quad (3)$$

$$R_{avg} = r = 1.23 \cdot \frac{\lambda}{2\sin\theta}. \quad (4)$$

Through Eq. 1 to Eq. 4, there are two points worth noting: the first one is that the scattered intensity is closely related to interatomic distance; the second is that Eq. 4 can be used to compute R_{avg} by the term $\lambda/(2\sin\theta)$ multiplied by a factor, e.g., 1.23. As this factor is derived on the assumption that atoms of one type are randomly packed, it is still questionable whether it is transferable to the real amorphous metallic systems. Indeed, shortly after this model was proposed, this question was investigated on some liquid metals and polymers, and it was found that in practice the factor has a smaller value of 1.1 to 1.2 among these materials [9]. As currently a large number of metallic glasses have been developed, it is interesting to look at this question again, i.e., whether it is applicable to metallic glasses since their compositions are usually complicated.

3. MATERIALS AND METHODS

Several of amorphous compositions were fabricated in-house, with the details of the fabrication methods already presented in our previous work [10]. In addition, a La-based MG was obtained from Jiang's group, the fabrication method of which has been reported elsewhere [11]. The full range of MGs used in this work are listed in Table 1 along with literature values for their physical quantities. R_{Bragg} is a radius calculated from the Bragg equation $\lambda/(2\sin\theta)$, while R_{avg} is a weighted average and defined as $R_{avg}=\sum w_{ij} r_{ij}$ (w_{ij} is the weight factor and r_{ij} is the atom-pair distance).

The X-ray diffraction (XRD) was operated on a system (Philips X'pert 1830) using monochromatic Cu *K*α radiation (λ = 0.1542 nm). The step size was 0.02° with a scan rate of 1.00°/min. The working voltage and current were respectively maintained at 30 kV and 20 mA.

In Table 1, the atomic packing efficiency (AFE) was calculated according to the equations below:

$$\mathrm{AFE} = \rho N_A V/M; \quad (5)$$

$$V = \sum c_i v_i = \sum c_i \frac{4}{3}\pi r_i^3; \quad (6)$$

$$M = \sum c_i M_i, \quad (7)$$

where ρ is the mass density; V is the molecular volume; M is the molar mass of the molecule; M_i is the atomic mass; N_A is the Avogadro constant; c_i is the molar fraction of atom i; v_i the volume of atom i, r_i is the atomic radius.

4. RESULTS AND DISCUSSION

Fig. 1 shows the XRD spectra for some compositions of this study. Over the whole range of diffraction angle, no crystalline peaks appear. A broad diffraction peak typically occurs, which is characteristic of an amorphous structure. To obtain the diffraction angle at the maximum intensity, the background was first subtracted, and then the broad peak was fitted by a Voigt function [12]. A standard error less than 0.1° was usually met, and thus the influence of the fitting uncertainty could be neglected on the calculation of R_{Bragg}. The diffraction angle where the broad peak emerges depends on the composition; for example, in Fig. 1 a, La-based MG has an angle of 31.12°, while the other samples have an angle of close to 38°. Interestingly, in Fig. 1 b, the diffraction halo maximum for Cu_xZr_{100-x} thin films shifts to the high-angle side as the Cu content increases.

Table 1. Summary of data on physical properties of various MGs (R_{Bragg} is usually measured with Cu *K*α X-ray radiation)

Composition	Density, g/cm^3	Atomic packing efficiency	Shear modulus, GPa	Poisson's ratio	R_{Bragg}	R_{avg}	R_{avg} / R_{Bragg}	Reference
Metal-Metal								
$Al_{86.5}Ni_{4.5}Y_9$	3.103	0.698	27		2.37	2.90	1.22	This work & [13, 14]
$Ca_{60}Mg_{15}Zn_{25}$	2.289	0.678			2.80	3.34	1.19	[6, 15]
$Ca_{65}Mg_{15}Zn_{20}$	2.05	0.654	10.3	0.306				[16, 17]
$Ca_{50}Mg_{20}Zn_{30}$	2.59	0.70			2.63	2.95	1.12	[18]
$Ce_{70}Al_{10}Cu_{20}$	6.4	0.697	11.3	0.329				[19]
$Cu_{50}Zr_{50}$	7.33	0.710	30	0.36	2.34	2.87	1.23	This work & [20, 21]
$Cu_{59.7}Zr_{40.3}$	7.66	0.720			2.25	2.76	1.23	This work & [22, 23]
$Cu_{57.5}Hf_{27.5}Ti_{15}$	9.91	0.717	37.3	0.356				[16, 24]
$La_{65}Al_{14}(Cu_{5/6}Ag_{1/6})_{11}Ni_5Co_5$	6.12	0.737	14.5	0.365	2.87	3.46	1.21	This work & [11]
$Mg_{65}Cu_{25}Y_{10}$	3.28	0.712	18.9	0.329	2.37	2.93	1.24	[25, 26]
$Mg_{67}Zn_{28}Ca_5$	2.983	0.662	17.3		2.40	2.95	1.23	This work & [27, 28]
$Zr_{67}Ni_{33}$	7.06	0.742	28		2.47	3.05	1.23	[29]
$Zr_{45}Cu_{45}Al_{10}$	7.204	0.742	35.4	0.359				[16, 30]
Metal-Metalloid								
$Fe_{80}B_{20}$	7.31	0.699	65		2.02	2.52	1.25	[31, 32]
$Ni_{80}P_{20}$	7.9	0.718	36.7	0.394	2.01	2.44	1.21	[33, 34]
$Pd_{77.5}Cu_6Si_{16.5}$	10.4	0.704	31.8	0.410	2.23	2.75	1.23	[35, 36]
$Pd_{40}Cu_{40}P_{20}$	9.3	0.721	33.2	0.402	2.17	2.67	1.23	[37, 38]
$Pd_{40}Cu_{30}Ni_{10}P_{20}$	9.28	0.674	34.5					[39, 40]

According to Eq. 4, this peak shift with the addition of Cu corresponds to a decrease in the average bonding length R_{avg}, which is attributed to the smaller size of Cu atoms than that of Zr atoms. A similar peak shift has been observed in systems with strong chemical interaction, such as Zr-Ti melts [41]. The values of R_{avg} for various compositions are summarized in Table 1.

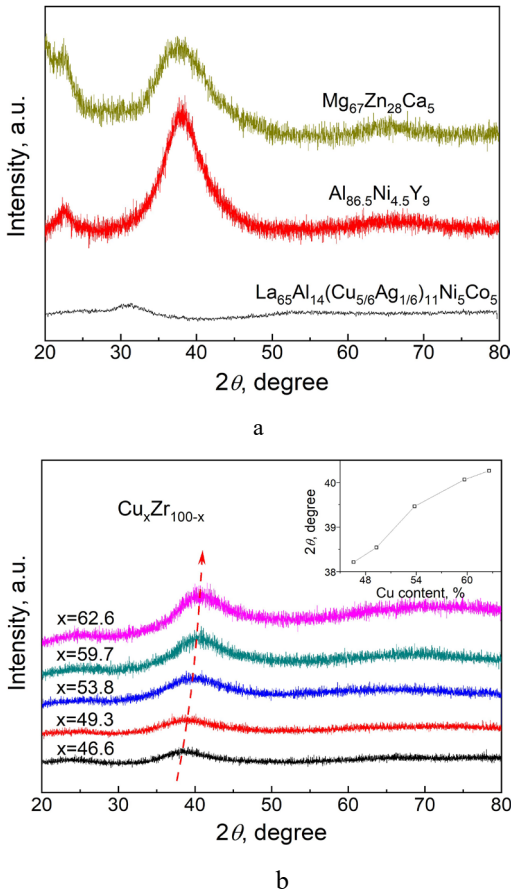

Fig. 1. X-ray diffraction patterns: a – $Mg_{67}Zn_{28}Ca_5$, $Al_{86.5}Ni_{4.5}Y_9$ and $La_{65}Al_{14}(Cu_{5/6}Ag_{1/6})_{11}Ni_5Co_5$; b – Cu_xZr_{100-x} with an inset of Diffraction angle vs Cu content

The factors of some MGs are listed in Table 1. It should be noted that, as the factor is computed by dividing R_{Bragg} by R_{avg}, care must be taken to measure R_{Bragg} and R_{avg}. Regarding R_{Bragg}, it can be easily derived from a conventional X-ray diffraction pattern of the amorphous alloy; regarding R_{avg}, its derivation is somewhat complicated because the total pair distribution function (PDF) has to be measured at first, and then its first peak is deconvolved into partial ones (as shown in Fig. 2). The dotted curves indicate the experimental PDFs, and the red solid curves represent the fitting PDFs. At the bottom of each figure are the partial PDFs in color, which are derived from the deconvolution of the experimental PDFs. For MGs are isotropic systems, the partial peaks, which correspond to the respective atom-pairs, can be described by the Gaussian function [42]. The challenge lies in the fact that the atomic pair length is unknown. There are two ways to solve the problem: one is to refer to the literature as listed in Table 1; the other is to fit the experimental PDF.

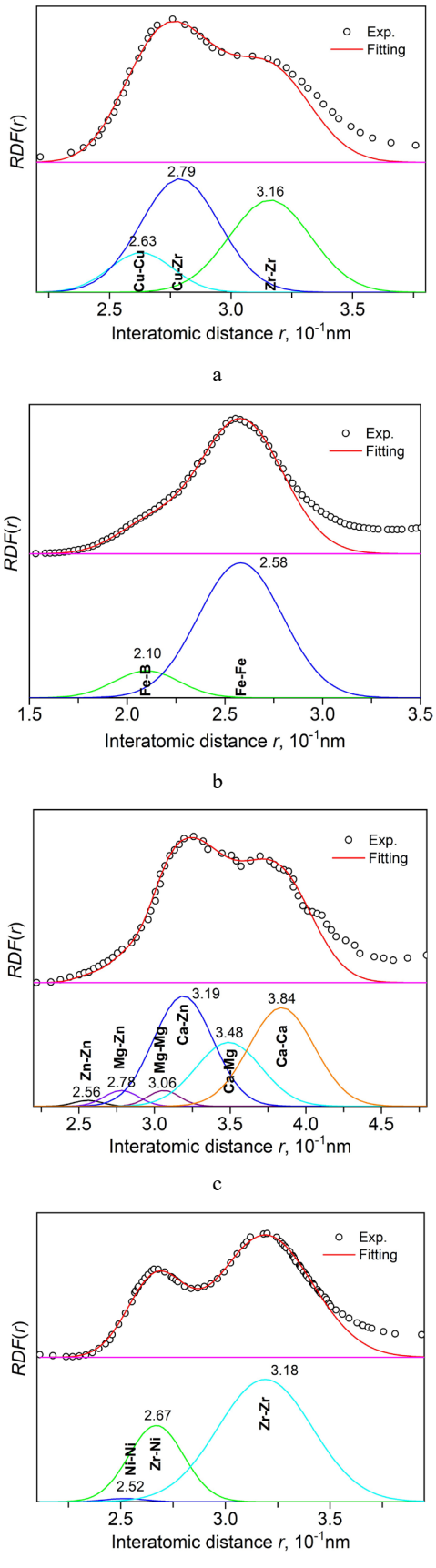

Fig. 2. Pair distribution functions (PDFs) for various metallic glasses: a – $Cu_{50}Zr_{50}$ [43]; b – $Fe_{80}B_{20}$ [44]; c – $Ca_{60}Mg_{15}Zn_{25}$ [6]; d – $Zr_{67}Ni_{33}$ [45]

For PDF fitting, a good starting point is to use the assessed atomic radii [46] for determining the initial atom-pair distance. Specifically, the main peak is split into Gaussian sub-peaks; the position, width, and height of sub-peaks are adjusted so that the difference between the calculated PDF and experimental one is reduced to a minimum.

The area fraction of each atomic pair is presented in Table 2. Obviously, they are approximately equal to the weight factors, indicating that the simulation of PDF is satisfactory. The deviation of fitting PDFs from experimental ones on the right sides is due to the contribution from the secondary nearest-neighbour shell [47]. From Table 1, most of the MGs have a value slightly different from that predicted by Eq. 4, implying that their atomic structures could deviate from the random packing model. The deviation is understandable because the random packing model does not take into account the chemical short-range order. For MGs containing multiple elements, unlike atoms, usually have an interaction different from like ones, leading to the change of local atomic configuration, and then the change of the first peak position [48].

Fig. 3 shows the relationship between R_{Bragg} and R_{avg}, to which a linear function of gradient of 1.22 has been fitted.

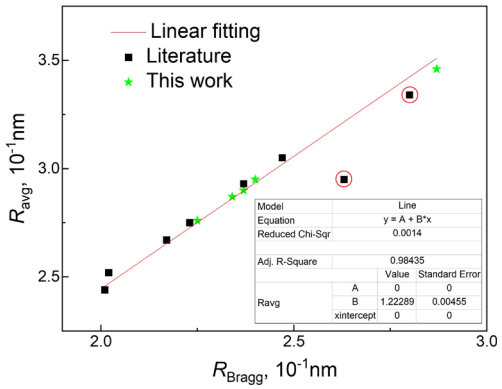

Fig. 3. Relationship between average interatomic distance R_{avg} and Bragg radius R_{Bragg}

It is known that the close packed face-centered cubic (fcc) lattice has such a ratio between the gap of closest lattice plane (111) and the atomic spacing. The coincidence indicates that the amorphous alloys have a dense packing structure. This statement is in agreement with literature reports that bulk metallic glasses (BMGs) usually have a density close to their crystalline counterparts [49, 50]. Nevertheless, it can be observed that two of the MGs in Fig. 3 appear to stay further away from the linear fitting line (as indicated by open circles), and both these alloys are Ca-based. The reason for their deviation is attributed to the bonding nature. As reported by Senkov et al. [6], in Ca-based MGs, the bonding between Ca and Mg is typically covalent, while for other MGs, metallic bonding is dominant.

According to Eq. 4, an ideal random packing structure has a factor of 1.23, and it is also known that the ideal random packing efficiency is about 0.64. In consideration of these facts, it is interesting to note if there is a relationship between atomic packing density and the factor. Based on the data in Table 1, the ratio R_{avg}/R_{Bragg} is plotted against the atomic packing efficiency in Fig. 4. Two types of MGs can be readily identified: one is enclosed in the ellipse zone (named as Type I, the ellipse is a Pearson ellipse with a confidence 90 %) and the other is outside of this region (named as Type II).

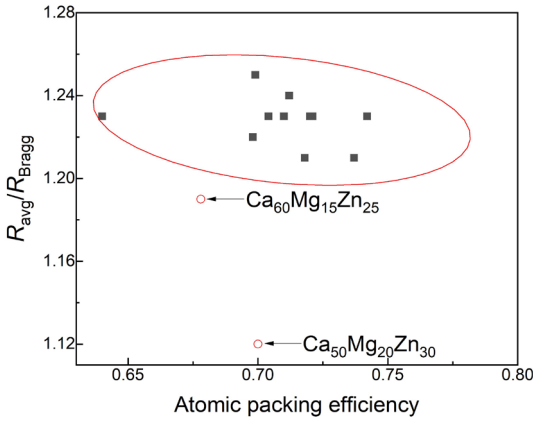

Fig. 4. Dependence of ratio R_{avg}/R_{Bragg} on atomic packing efficiency. The ellipse in red is a Pearson ellipse with a confidence 90 %. The red circles indicate Ca-based MGs, which have a covalent-bonding character

Table 2. Summary of weight factors for some metallic glasses. R_{avg} is obtained by multiplying the atomic pair distance by its respective weight factors and summing them up

Composition	X-ray wavelength, nm	Weight factor		Area fraction	Reference
$Cu_{50}Zr_{50}$	0.0125	W_{CuCu}	0.177	0.132	[20, 43]
		$2W_{CuZr}$	0.487	0.472	
		W_{ZrZr}	0.336	0.396	
$Fe_{80}B_{20}$	*	W_{FeFe}	0.904	0.866	[44]
		$2W_{FeB}$	0.094	0.134	
$Ca_{60}Mg_{15}Zn_{25}$	0.05599 (Ag K_α)	W_{CaCa}	0.317	0.352	[6]
		$2W_{CaMg}$	0.094	0.227	
		$2W_{CaZn}$	0.397	0.355	
		W_{MgMg}	0.007	0.028	
		$2W_{MgZn}$	0.059	0.029	
		W_{ZnZn}	0.124	0.009	
$Zr_{67}Ni_{33}$	0.013	W_{ZrZr}	0.553	0.729	[45]
		$2W_{ZrNi}$	0.381	0.262	
		W_{NiNi}	0.066	0.009	

Further analysis shows that Type I encompasses those alloys where metallic bonds dominates, while Type II mainly consists of covalent bonding pairs. The alloys of Type I have a factor that is dependent on atomic packing efficiency, i.e., the larger the packing density and the smaller the ratio; although this dependence is small, it is not negligible.

Again, like the behavior presented in Fig. 3, the alloys with covalent bonds remain outside of the encircled region. The discrepancy is considered to lie in the different atomic arrangement in the first coordination shell. As has been explored by Cheng and Ma [51], the atomic bonding distance is the key factor governing the atomic configuration of the first shell (the configuration is characterized by coordination number, coordination polyhedral, and size). When the bonding nature switches from metallic to covalent, a shortening of the interatomic distance can be expected, and thus a change of the short-range atomic structure is induced. In Ca-based MGs as quoted in Table 1, the majority of atom pairs are either Ca-Ca, Ca-Mg or Ca-Zn, in which the interatomic distances are shorter than their respective metallic bonds due to the absence of long-range order [6]. Although this shortening exists in other MGs shown in Table 1, such as $Fe_{80}B_{20}$ (Fe-B atom pair is partially covalent [51]), the Fe-Fe atom pair (where the interatomic distance is close to the addition of the metallic radii) is present in a large amount at the first shell (See Fig. 2 b) so that the total metallic bonding is significant.

Between $Ca_{60}Mg_{15}Zn_{25}$ and $Ca_{50}Mg_{20}Zn_{30}$, the latter has a smaller correction factor. The reason is hidden in the skew normal distribution of the PDF first peak, as shown in Fig. 2. The skewness is attributed to the anharmonic and asymmetric interaction between atoms, and thus atoms at low r side are harder to spread than those at large r side [48]. Since $Ca_{50}Mg_{20}Zn_{30}$ has more Zn and Mg atoms, the fraction of Ca-Mg and Ca-Zn pairs increases, and its first peak position is expected to shift to the lower r side as both pairs have a length shorter than Ca-Ca. The peak position is relevant to the weighted average R_{avg} as discussed in the 'Theory' section, but not a good estimate of the mean bond length because of the skewness [52]. The effect of the mean bond length on the correction factor is left for future work.

4. CONCLUSIONS

The amorphous structure of metallic glasses is dependent on composition. In real amorphous alloys with predominantly metallic bonds, the distance between nearest neighbouring atoms is related to the Bragg equation $\lambda/(2\sin\theta)$ by a factor of 1.22, slightly lower than predicted by the Debye equation. The lower factor is due to denser atomic packing. Further evidence for this was seen with two Ca-based MGs, where the covalent bonding character leads to shorter interatomic distances and thus an even smaller factor. The findings could provide confidence to estimate the average interatomic distance using the conventional XRD data.

Acknowledgments

This work was supported by the Natural Science Foundation of Zhejiang Province [Grant No. LY21E010001]; the Program of 'Xinmiao' (Potential) Talents in Zhejiang Province [No. 2024R423A004]; Liaoning Key Laboratory of Metal Matrix Composites Open Fund Project (2023); the Scientific Research Foundation of Zhejiang University of Water Resources and Electric Power (JBGS2025013).

REFERENCES

1. **Tong, Y., Dmowski, W., Bei, H., Yokoyama, Y., Egami, T.** Mechanical Rejuvenation in Bulk Metallic Glass Induced by Thermo-Mechanical Creep *Acta Materialia* 148 2018: pp. 384 – 390. https://doi.org/10.1016/j.actamat.2018.02.019
2. **Dyakova, V., Stefanov, G., Marinkov, N., Gyurov, S., Kostova, Y.** Rheological Behavior of a New Amorphous Alloy $(Al_{74}Cu_{16}Mg_{10})_{99.7}Zr_{0.3}$ *Materials Science (Medžiagotyra)* 30 2024: pp. 177 – 182. https://doi.org/10.1016/10.5755/j02.ms.34241
3. **Louzguine-Luzgin, D.V.** Structural Changes in Metallic Glass-Forming Liquids on Cooling and Subsequent Vitrification in Relationship with Their Properties *Materials* 15 2022: pp. 7285. https://doi.org/10.3390/ma15207285
4. **Liu, Y., Hu, S., Luo, J., Hu, H., Huang, X.** Investigation of Medium Range Order Defects in Cu_xZr_{100-x} (x = 50, 56, 60, 64) Metallic Glasses Using Reverse Monte Carlo Modeling *Metals* 13 2023: pp. 70. https://doi.org/10.3390/met13010070
5. **Senkov, O.N., Scott, J.M., Miracle, D.B.** Composition Range and Glass Forming Ability of Ternary Ca-Mg-Cu Bulk Metallic Glasses *Journal of Alloys and Compounds* 424 2006: pp. 394 – 399. https://doi.org/10.1016/j.jallcom.2006.01.104
6. **Senkov, O.N., Miracle, D.B., Barney, E.R., Hannon, A.C., Cheng, Y.Q., Ma, E.** Local Atomic Structure of Ca-Mg-Zn Metallic Glasses *Physical Review B* 82 2010: pp. 104206. https://doi.org/10.1103/PhysRevB.82.104206
7. **Evertz, S., Prünte, S., Patterer, L., Marshal, A., Holzapfel, D.M., Schökel, A., Hans, M., Primetzhofer, D., Schneider, J.M.** Boron Concentration Induced Co-Ta-B Composite Formation Observed in the Transition from Metallic to Covalent Glasses *Condensed Matter* 5 2020: pp. 18. https://doi.org/10.3390/condmat5010018
8. **Klug, H.P., Alexander, L.E.** X-ray Diffraction Procedures for Polycrystalline and Amorphous Materials (2nd edition). John Wiley & Sons, New York, 1974.
9. **Guinier, A.** X-ray Diffraction in Crystals, Imperfect Crystals, and Amorphous Bodies. Dover Publications, Inc., New York, 1994.
10. **Pang, J., Wang, Y., Tan, M.J., Liew, K.M.** Thermal Properties of Metallic Glasses: Heating Rate Dependence and Their Correlation *Materials Letters* 126 2014: pp. 81 – 84. https://doi.org/10.1016/j.matlet.2014.03.158
11. **Jiang, Q.K., Zhang, G.Q., Yang, L., Wang, X.D., Saksl, K., Franz, H., Wunderlich, R., Fecht, H., Jiang, J.Z.** La-based Bulk Metallic Glasses with Critical Diameter up to 30mm *Acta Materialia* 55 2007: pp. 4409 – 4418. https://doi.org/10.1016/j.actamat.2007.04.021

12. **Suortti, P., Ahtee, M., Unonius, L.** Voigt Function Fit of X-ray and Neutron Powder Diffraction Profiles *Applied Crystallography* 12 1979: pp. 365 – 369. https://doi.org/10.1107/S002188987901270X
13. **Yan, M., Kohara, S., Wang, J.Q., Nogita, K., Schaffer, G.B., Qian, M.** The Influence of Topological Structure on Bulk Glass Formation in Al-based Metallic Glasses *Scripta Materialia* 65 2011: pp. 755 – 758. https://doi.org/10.1016/j.scriptamat.2011.07.009
14. **Kuball, A., Stolpe, M., Busch, R.** Crystallization Behavior of the $Al_{86}Ni_8Y_6$ Metallic Glass Forming Alloy upon Rapid Cooling *Journal of Alloys and Compounds* 737 2018: pp. 398 – 404. https://doi.org/10.1016/j.jallcom.2017.12.044
15. **Carow-Watamura, U., Louzguine, D., Takeuchi, A.** Physical Properties of Ternary Amorphous Alloys. Part 2: Systems from B-Be-Fe to Co-W-Zr. Springer, Berlin Heidelberg, 2011: pp. 414 – 423.
16. **Pang, J.J., Tan, M.J., Liew, K.M.** On Valence Electron Density, Energy Dissipation and Plasticity of Bulk Metallic Glasses *Journal of Alloys and Compounds* 577 2013: pp. S56 – S65. https://doi.org/10.1016/j.jallcom.2012.03.036
17. **Liu, B.B., Hu, L., Wang, Z.Y., Ye, F.** Viscosity, Relaxation and Fragility of the $Ca_{65}Mg_{15}Zn_{20}$ Bulk Metallic Glass *Intermetallics* 109 2019: pp. 8 – 15. https://doi.org/10.1016/j.intermet.2019.03.002
18. **Egami, T., Poon, S.J., Zhang, Z., Keppens, V.** Glass transition in metallic glasses: A microscopic model of topological fluctuations in the bonding network *Physical Review B* 76 2007: pp. 024203. https://doi.org/10.1103/PhysRevB.76.024203
19. **Li, D., Chen, H., Qu, B., Zhou, R., Zhang, F., Zhang, B.** Micro-alloying Effects of Co on Structural and Dynamic Properties of CeAlCu Glass-forming Melts by ab initio Molecular Dynamics Simulations *Journal of Non-Crystalline Solids* 572 2021: pp. 121109. https://doi.org/10.1016/j.jnoncrysol.2021.121109
20. **Mattern, N., Jóvári, P., Kaban, I., Gruner, S., Elsner, A., Kokotin, V., Franz, H., Beuneu, B., Eckert, J.** Short-Range Order of Cu–Zr Metallic Glasses *Journal of Alloys and Compounds* 485 2009: pp. 163 – 169. https://doi.org/10.1016/j.jallcom.2009.05.111
21. **Li, D., Zhou, J., Chen, H., Qu, B., Zhou, R.** Size Effects on the Structural and Physical Properties of $Cu_{50}Zr_{50}$ Metallic Glass Nanoparticles *Physica E: Low-dimensional Systems and Nanostructures* 145 2023: pp. 115502. https://doi.org/10.1016/j.physe.2022.115502
22. **Mattern, N., Schöps, A., Kühn, U., Acker, J., Khvostikova, O., Eckert, J.** Structural Behavior of Cu_xZr_{100-x} Metallic Glass (x=35−70) *Journal of Non-Crystalline Solids* 354 2008: pp. 1054 – 1060. https://doi.org/10.1016/j.jnoncrysol.2007.08.035
23. **Sun, Y.L., Shen, J., Valladares, A.A.** Atomic Structure and Diffusion in $Cu_{60}Zr_{40}$ Metallic Liquid and Glass: Molecular Dynamics Simulations *Journal of Applied Physics* 106 2009: pp. 073520. https://doi.org/10.1063/1.3245324
24. **Chen, M.** Mechanical Behavior of Metallic Glasses: Microscopic Understanding of Strength and Ductility *Annual Review of Materials Research* 38 2008: pp. 445 – 469. https://doi.org/10.1146/annurev.matsci.38.060407.130226
25. **Uhlenhaut, D.I., Dalla Torre, F.H., Castellero, A., Gomez, C.A.P., Djourelov, N., Krauss, G., Schmitt, B., Patterson, B., Löffler, J.F.** Structural Analysis of Rapidly Solidified Mg–Cu–Y Glasses during Room-temperature Embrittlement *Philosophical Magazine* 89 2009: pp. 233 – 248. https://doi.org/10.1080/14786430802603720
26. **Liu, W., Johnson, W.L.** Precipitation of BCC Nanocrystals in Bulk Mg–Cu–Y Amorphous Alloys *Journal of Materials Research* 11 1996: pp. 2388 – 2392. https://doi.org/10.1557/JMR.1996.0302
27. **Ju, S.P., Huang, H.H., Huang, J.C.C.** Predicted Atomic Arrangement of $Mg_{67}Zn_{28}Ca_5$ and $Ca_{50}Zn_{30}Mg_{20}$ Bulk Metallic Glasses by Atomic Simulation *Journal of Non-Crystalline Solids* 388 2014: pp. 23 – 31. https://doi.org/10.1016/j.jnoncrysol.2014.01.005
28. **Erkartal, M., Durandurdu, M.** An In-depth Investigation of Mg-Zn-Ca Metallic Glasses: A First Principles Study *Computational Materials Science* 153 2018: pp. 326 – 337. https://doi.org/10.1016/j.commatsci.2018.07.013
29. **Mihailov, L., Spassov, T., Bojinov, M.** Effect of Microstructure on the Electrocatalytic Activity for Hydrogen Evolution of Amorphous and Nanocrystalline Zr–Ni Alloys *International Journal of Hydrogen Energy* 37 2012: pp. 10499 – 10506. https://doi.org/10.1016/j.ijhydene.2012.04.042
30. **Yu, P., Bai, H.Y.** Poisson's Ratio and Plasticity in CuZrAl Bulk Metallic Glasses *Materials Science and Engineering: A* 485 2008: pp. 1 – 4. https://doi.org/10.1016/j.msea.2007.07.062
31. **Hirata, A., Hirotsu, Y.** Structure Analyses of Fe-based Metallic Glasses by Electron Diffraction *Materials* 3 2010: pp. 5263 – 5273. https://doi.org/10.3390/ma3125263
32. **Ma, L., Wang, L., Zhang, T., Inoue, A.** Effect of Zr and Nb Elements on Glass Forming Ability of Fe-B Alloy *Acta Metallurgica Sinica* 6 1999: pp. 631 – 633.
33. **Sheng, H.W., Luo, W.K., Alamgir, F.M., Bai, J.M., Ma, E.** Atomic Packing and Short-to-Medium-Range Order in Metallic Glasses *Nature* 439 2006: pp. 419 – 425. https://doi.org/10.1038/nature04421
34. **Huang, Q.S., Lu, B.F., Kong, L.T., Li, J.F.** On the Glass-Forming Ability of Ni–P Binary Alloys *Materials Research Bulletin* 47 2012: pp. 1973 – 1977. https://doi.org/10.1016/j.materresbull.2012.04.016
35. **Kajita, S., Kohara, S., Onodera, Y., Fukunaga, T., Matsubara, E.** Structural Analysis of Pd-Cu-Si Metallic Glassy Alloy Thin Films with Varying Glass Transition Temperature *Materials Transactions* 52 2011: pp. 1349 – 1355. https://doi.org/10.2320/matertrans.M2011023
36. **Shao, Y., Yang, G., Yao, K.** Nanocrystalline Phase Formation inside Shear Bands of Pd-Cu-Si Metallic Glass *Advances in Materials Science and Engineering* 2014 2014: pp. 490181. https://doi.org/10.1155/2014/490181
37. **Hosokawa, S., Sato, H., Ichitsubo, T., Nakatake, M., Happo, N., Bérar, J.F., Boudet, N., Usuki, T., Pilgrim, W.C., Matsubara, E., Nishiyama, N.** Inhomogeneity and Glass-forming Ability in the Bulk Metallic Glass $Pd_{42.5}Ni_{7.5}Cu_{30}P_{20}$ as Seen via X-ray Spectroscopies *Physical Review B* 80 2009: pp. 174204. https://doi.org/10.1103/PhysRevB.80.174204
38. **Nishiyama, N., Inoue, A.** Glass-Forming Ability of Bulk $Pd_{40}Ni_{10}Cu_{30}P_{20}$ Alloy *Materials Transactions, JIM* 37 1996: pp. 1531 – 1539. https://doi.org/10.2320/matertrans1989.37.1531

39. **Xiong, J., Wang, H., Zhang, G., Chen, Y., Ma, J., Mo, R.** Machinability and Surface Generation of $Pd_{40}Ni_{10}Cu_{30}P_{20}$ Bulk Metallic Glass in Single-Point Diamond Turning *Micromachines* 11 2020: pp. 4. https://doi.org/10.3390/mi11010004
40. **Mattern, N., Bednarcik, J., Liermann, H.-P., Eckert, J.** Structural Behaviour of $Pd_{40}Cu_{30}Ni_{10}P_{20}$ Metallic Glass under High Pressure *Intermetallics* 38 2013: pp. 9 – 13. https://doi.org/10.1016/j.intermet.2013.02.019
41. **Zhang, C., Feng, Y., Liu, H., Szabó, S., Holland-Moritz, D., Evenson, Z., Yang, F., Peng, H.** Local Structures and Undercooling Ability of Zr-Ti Melts *Journal of Non-Crystalline Solids* 613 2023: pp. 122348. https://doi.org/10.1016/j.jnoncrysol.2023.122348
42. **Dimitrov, D., Röder, H., Bishop, A.** Peak Positions and Shapes in Neutron Pair Correlation Functions from Powders of Highly Anisotropic Crystals *Physical Review B* 64 2001: pp. 014303. https://doi.org/10.1103/PhysRevB.64.014303
43. **Georgarakis, K., Yavari, A.R., Louzguine-Luzgin, D.V., Antonowicz, J., Stoica, M., Li, Y., Satta, M., LeMoulec, A., Vaughan, G., Inoue, A.** Atomic Structure of Zr-Cu Glassy Alloys and Detection of Deviations from Ideal Solution Behavior with Al Addition by X-ray Diffraction Using Synchrotron Light in Transmission *Applied Physics Letters* 94 2009: pp. 191912. https://doi.org/10.1063/1.3136428
44. **Hirata, A., Hirotsu, Y., Matsubara, E.** Local Atomic Structures of Amorphous $Fe_{80}B_{20}$ and $Fe_{70}Nb_{10}B_{20}$ Alloys Studied by Electron Diffraction *Materials Transactions* 46 2005: pp. 2781 – 2784. https://doi.org/10.2320/matertrans.46.2781
45. **Georgarakis, K., Yavari, A., Aljerf, M., Louzguine-Luzgin, D., Stoica, M., Vaughan, G., Inoue, A.** On the Atomic Structure of Zr-Ni and Zr-Ni-Al Metallic Glasses *Journal of Applied Physics* 108 2010: pp. 023514. https://doi.org/10.1063/1.3446131
46. **Miracle, D., Louzguine-Luzgin, D., Louzguina-Luzgina, L., Inoue, A.** An Assessment of Binary Metallic Glasses: Correlations between Structure, Glass Forming Ability and Stability *International Materials Reviews* 55 2010: pp. 218 – 256. https://doi.org/10.1179/095066010X12646898728200
47. **Hufnagel, T., Ott, R., Almer, J.** Structural Aspects of Elastic Deformation of a Metallic Glass *Physical Review B-Condensed Matter and Materials Physics* 73 2006: pp. 064204. https://doi.org/10.1103/PhysRevB.73.064204
48. **Ding, J., Ma, E.** Computational Modeling Sheds Light on Structural Evolution in Metallic Glasses and Supercooled Liquids *NPJ Computational Materials* 3 2017: pp. 9. https://doi.org/10.1038/s41524-017-0007-1
49. **Miracle, D.B., Sanders, W.S., Senkov, O.N.** The Influence of Efficient Atomic Packing on the Constitution of Metallic Glasses *Philosophical Magazine* 83 2003: pp. 2409 – 2428. https://doi.org/10.1080/1478643031000098828
50. **Guo, G.** Quasi-Icosahedral Clusters in Zr-Based Metallic Glasses *Metals* 10 2020: pp. 1135. https://doi.org/10.3390/met10091135
51. **Cheng, Y., Ma, E.** Atomic-Level Structure and Structure-Property Relationship in Metallic Glasses *Progress in Materials Science* 56 2011: pp. 379 – 473. https://doi.org/10.1016/j.pmatsci.2010.12.002
52. **Sukhomlinov, S.V., Müser, M.H.** Determination of Accurate, Mean Bond Lengths from Radial Distribution Functions *The Journal of Chemical Physics* 146 2017: pp. 024506. https://doi.org/10.1063/1.4973804